The "Inactive" Eddy Motion and the Large-Scale Turbulent Pressure Fluctuations in the Dynamic Sublayer

GABRIEL G. KATUL,*,+ JOHN D. ALBERTSON,@ CHENG-I HSIEH,* PAUL S. CONKLIN,* JOHN T. SIGMON,* MARC B. PARLANGE,@ AND KEN R. KNOERR*

*School of the Environment, Duke University, Durham, North Carolina
+ Center for Hydrologic Sciences, Duke University, Durham, North Carolina
@ Hydrologic Science, University of California, Davis, California

(Manuscript received 20 March 1995, in final form 16 February 1996)

ABSTRACT

The statistical structure of the turbulent pressure fluctuations was measured in the dynamic sublayer of a large grass-covered forest clearing by a free air static pressure probe and modeled using Townsend's hypothesis. Townsend's hypothesis states that the eddy motion in the equilibrium layer can be decomposed into an active component, which is only a function of the ground shear stress and height, and an inactive component, which is produced by turbulence in the outer region. It is demonstrated that the inactive eddy motion contributes significantly to the pressure and longitudinal velocity power spectra for wavenumbers much smaller than that corresponding to the height above the ground surface. Because of the importance of this inactive eddy motion contribution, it was possible to derive and validate a scaling law for the pressure power spectrum at low wavenumbers. The root-mean-square pressure was derived from the ground shear stress using simplifications to the Poisson equation that relate the Laplacian of the pressure fluctuations to the divergence of momentum. The theoretically derived and experimentally measured root-mean-square pressure values were in close agreement with other theoretical predictions and numerous laboratory measurements for wall pressure fluctuations. The relation between the root-mean-square pressure and the ground shear stress was also used to determine the similarity constant for the large-scale pressure spectrum. From considerations of the integral representation of the Poisson equation, previous laboratory measurements, and the present data, it was shown that this similarity constant does not vary appreciably with the roughness of the boundary layer. Finally, it was demonstrated that the inactive eddy motion does not contribute to the vertical velocity power spectrum in agreement with Monin and Obukhov surface-layer similarity theory.

1. Introduction

The turbulent pressure fluctuations in the atmospheric surface layer (ASL) play a central role in turbulent transport processes and in land–atmosphere interactions. Interest in turbulent pressure fluctuations is motivated by the role of 1) the pressure transport term in the turbulent kinetic energy (TKE) budget equation (e.g., Wyngaard and Cote 1971; McBean and Elliott 1975, 1978; Högström 1990), 2) the pressure gradients in linking small- and large-scale organized motion (e.g., Snarski and Lueptow 1995; Schols and Wartena 1986; Thomas and Bull 1983), and 3) the pressure fluctuations in air movement and dispersion within the lower parts of forest canopies (e.g., Sigmon et al. 1983; Shaw and Zhang 1992; Conklin 1994).

The statistical structure of the turbulent static pressure fluctuations is less understood than most other ASL flow variables (e.g., velocity or scalar fluctuations). This is, in part, due to the limited number of static pressure fluctuation experiments (hereafter referred to as free air static pressure measurements) carried out in the ASL. The difficulty in measuring static pressure fluctuations is attributed to the close coupling between static pressure and velocity so that changes in velocity caused by inserting a pressure probe will contaminate the measured static pressure with dynamic pressure effects (Wyngaard et al. 1994).

It is typically assumed that turbulent velocity statistics in the inner and outer regions of the atmospheric boundary layer (ABL) are universal functions of a limited number of dynamical variables (see Raupach et al. 1991 for review). An equivalent approach for the pressure fluctuations has not been formulated. The lack of a similarity theory for the pressure fluctuations may be attributed to the form of the Poisson equation. For incompressible turbulent flows, the static pressure is related to the velocity fluctuations through a Poisson equation derived from the divergence of the momentum balance. The solution to this Poisson equation at a point requires knowledge of the velocity components at all

Corresponding author address: Dr. Gabriel G. Katul, School of the Environment, Duke University, Box 90328, Durham, NC 27708-0328.

points in the flow domain. In general, the turbulent velocity components cannot be determined at all points, thus limiting comprehensive theoretical treatments.

Despite this difficulty, the success of the Batchelor–Obukhov theory (see Batchelor 1953; Hill and Wilczak 1995) in describing the spectrum of the small-scale static pressure fluctuations for a locally isotropic turbulent flow was well documented by George et al. (1984) and Conklin et al. (1991). Analogous power law formulations for the larger scales of motion, which are nonisotropic, are not well developed. In this study, the term large scale refers to scales much larger than the height above the ground surface (z) but much smaller than the mesoscales. The term small scale or fine scale refers to scales much smaller than z but much larger than the Kolmogorov microscale (η). For the latter, the velocity and static pressure spectra follow the well-known $-5/3$ and $-7/3$ inertial subrange power scaling proposed by Kolmogorov (1941) and Batchelor (1953), respectively.

The objective of this study is to construct approximate similarity formulation for the large-scale statistical properties of the pressure fluctuation in the near-neutral ASL (hereafter referred to as dynamic sublayer). The focus is restricted to the dynamic sublayer since 1) any complete theory for the pressure fluctuations in the ASL must match, in the limit, the near-neutral stratification; 2) the statistical structure of the velocity is well understood in that layer; and 3) the dynamic sublayer provides a good basis for comparisons with the numerous wind tunnel and other laboratory studies. The proposed similarity formulation is a combination of simplifications to the Poisson equation and extensions of Townsend's (1961) hypothesis regarding the respective roles of active and inactive eddy motion. The specific objectives are to derive analytical expressions for the pressure fluctuation power spectrum at small wavenumbers (large scales) and for the root-mean-square pressure fluctuations. The effects of active and inactive eddy motion in the dynamic sublayer of the ASL will also be considered for the longitudinal and vertical velocity for further support of Townsend's (1961) hypothesis. For that purpose, 10-Hz triaxial sonic anemometer velocity, free air static pressure, and water vapor density measurements were carried out at 1.54 m above the ground surface in a large grass-covered forest clearing at the Duke University Forest in Durham, North Carolina.

2. Theory

Here we will present the general equation describing the turbulent pressure fluctuations as function of velocity, invoke simplifications to identify the relevant scaling parameters for the static pressure fluctuations in the near-neutral ASL, and finally, investigate the importance of Townsend's (1961) hypothesis and Bradshaw's (1967) analysis. These arguments are used to derive the spectral properties of the large-scale static pressure fluctuations for the dynamic sublayer of the ASL. In order to independently verify specific assumptions related to the eddy motion and Townsend's (1961) hypothesis, the turbulent velocity field is also considered.

a. The general equation for static pressure fluctuations

Since our objective is to establish similarity relationships between the static pressure fluctuations and other ASL flow variables, a relationship between the static pressure and the velocity statistics is first discussed. Then Monin and Obukhov (1954) similarity (MOS) is used to describe the velocity, which in turn provides operational relationships between the static pressure statistics and other readily measured ASL flow variables. By taking the divergence of the Navier–Stokes (NS) equations

$$\frac{\partial U_i}{\partial x_i} = 0$$

$$\frac{\partial U_i}{\partial t} + U_j \frac{\partial U_i}{\partial x_j} = -\frac{\partial P}{\partial x_i} + \nu \frac{\partial^2 U_i}{\partial x_j \partial x_j} + \frac{g}{T}\delta_{i3}\theta, \quad (1)$$

we obtain the Poisson equation relating the static pressure to the velocity field

$$\frac{\partial^2 P}{\partial x_i \partial x_i} = -\frac{\partial^2 U_i U_j}{\partial x_i \partial x_j} + \frac{g}{T}\delta_{i3}\frac{\partial \theta}{\partial x_i}, \quad (2)$$

where U_i ($i = 1, 2, 3$) are the instantaneous velocity components, P is the kinematic static pressure (or pressure per unit density) departure from a hydrostatic reference state (Garratt 1992, 24–25), ν is the kinematic viscosity, T is the absolute mean kinetic temperature of the ASL, θ is the potential temperature, δ_{i3} is the Kroneker Delta, t is time, and x_i are the Cartesian coordinates. In this study, both meteorological and tensor notations ($U = U_1$, $V = U_2$, $W = U_3$; $x = x_1$, $y = x_2$, $z = x_3$) are used for velocity and position. The x_1 direction is aligned with the direction of the mean ground shear stress (τ_0).

Notice that the solution to the Poisson equation in (2) requires integration over the entire flow domain, and hence, the velocity field (i.e., $U_i U_j$) at all positions in the flow domain is needed to solve for P at x_i. This implies that P and $U_i U_j$ may not be locally related, and the velocity at very distant points can contribute to the pressure at x_i. Therefore, the pressure at a point need not be strongly correlated with the velocity at any one neighboring point.

The turbulent pressure fluctuations (p) can be derived following the usual Reynolds decomposition ($U_i = \langle U_i \rangle + u_i$; $P = \langle P \rangle + p$; $\theta = \langle \theta \rangle + \theta'$),

$$\frac{\partial^2 p}{\partial x_i \partial x_i} = -\frac{\partial^2}{\partial x_i \partial x_j}(u_i\langle U_j\rangle + u_j\langle U_i\rangle + u_i u_j - \langle u_i u_j\rangle) + \frac{g}{T}\frac{\partial \theta'}{\partial x_3}, \quad (3)$$

where $\langle U_i\rangle$ are the mean velocity components, u_i are the turbulent velocity fluctuations about $\langle U_i\rangle$ ($\langle u_i\rangle = 0$), $\langle P\rangle$ and p, $\langle\theta\rangle$ and θ' are the mean and turbulent fluctuating part of the pressure and potential temperature, respectively, and $\langle\cdot\rangle$ is the time-averaging operator assumed to converge to the ensemble-averaging operator by the ergodic hypothesis (see Monin and Yaglom 1971, 214–218).

In order to simplify (3), the approximate case where the turbulent flow is homogeneous in the mean in planes parallel to the ground surface for an ASL with negligible subsidence is considered so that

$$\frac{\partial^2 p}{\partial x_i \partial x_i} = -2\frac{\partial\langle U_1\rangle}{\partial x_3}\frac{\partial u_3}{\partial x_1} - \frac{\partial^2(u_i u_j - \langle u_i u_j\rangle)}{\partial x_i \partial x_j} + \frac{g}{T}\frac{\partial\theta'}{\partial x_3}. \quad (4)$$

$$= \text{(I)} \qquad + \text{(II)} \qquad + \text{(III)}$$

Therefore, p is influenced by three mechanisms in Eq. (4): I) the interaction of turbulence fluctuations normal to the ground surface with the mean shear, II) the interaction of turbulence with itself, and III) the thermal disturbances due to ground heating. In the dynamic sublayer, term III is much smaller than terms I and II and can be neglected.

b. *Scaling variables for the turbulent pressure fluctuations*

Kraichnan (1956a,b) suggested that the interaction of turbulence with the mean shear produces the major contribution to p close to the ground for an anisotropic and planar homogeneous turbulence. Panton and Linebarger (1974) found that 80% of the mean-square wall pressure fluctuation was produced by interaction of turbulence with the mean shear. Willmarth (1975) presented a comprehensive review of laboratory measurements supporting Kraichnan's (1956a) arguments regarding the relative importance of terms I and II for the ground pressure fluctuations. We note that the measurements by Corcos (1963, 1964) do not support Kraichnan's (1956a) arguments and conflict with later studies by Bull (1967), Bradshaw (1967), Blake (1970), and Thomas and Bull (1983). In the following analysis, Kraichnan's (1956a) result is adopted as a first approximation for arriving at an appropriate scaling term for p. Hence, in the dynamic sublayer, (4) simplifies to

$$\frac{\partial^2 p}{\partial x_i \partial x_i} = -2\frac{\partial\langle U_1\rangle}{\partial x_3}\frac{\partial u_3}{\partial x_1} = -2\left(\frac{u_*}{kz}\right)\frac{\partial u_3}{\partial x_1}, \quad (5)$$

where k (=0.4) is von Kármán's constant, u_* ($=[\tau_0/\rho]^{1/2}$) is the friction velocity, and ρ is the air density (see also Townsend 1976, 165–167). Hence, (5) demonstrates that Kraichnan's (1956a) argument results in a linear relation between the laplacian of the pressure fluctuations and the longitudinal gradient of the vertical velocity fluctuations in the dynamic sublayer. In order to relate the statistics of p in (5) to other ASL flow variables, dimensional considerations are considered next.

From Tennekes and Lumley (1972, p. 30), the appropriate normalizing variables for all instantaneous turbulence fluctuations are the root-mean-square amplitudes (rms). For p and u_i, the rms amplitudes are $\sigma_p = \langle p^2\rangle^{1/2}$, and $\sigma_{ui} = \langle u_i^2\rangle^{1/2}$ (where $\sigma_{u1} = \sigma_u$, $\sigma_{u2} = \sigma_v$, and $\sigma_{u3} = \sigma_w$). Therefore, the dimensionless variables for pressure (p_n), velocity (u_{in}), and length (x_{in}) are p/σ_p, u_i/σ_{ui}, and x_i/L_c, where L_c is a characteristic turbulence length scale. The characteristic length scale of the dynamic sublayer must be z ($=x_3$), and thus, the characteristic length scale of $\partial u_3/\partial x_1$ must be of order z (see, e.g., Yaglom 1979, 1993). The measurements by Bradshaw (1967) and Blake (1970) support this supposition and agree with the arguments presented by Hinze (1959, 500–502). Using these dimensionless variables,

$$\frac{\sigma_p}{z^2}\left[\frac{\partial^2 p_n}{\partial x_{i_n}\partial x_{i_n}}\right] = 2\frac{u_*}{kz}\frac{\sigma_{u_3}}{z}\left[\frac{-\partial u_{3_n}}{\partial x_{1_n}}\right]. \quad (6)$$

Since the dimensionless variables in square brackets on the left- and right-hand side of (6) must be of the same order of magnitude (see Panton 1984, chapter 8), then

$$\frac{\sigma_p}{z^2} \sim 2\frac{u_*}{kz}\frac{\sigma_{u_3}}{z}. \quad (7)$$

For the dynamic sublayer, it is well recognized that $\sigma_w = C_w u_*$, and, with $k = 0.4$ and $C_w = 1.2$ (Kader and Yaglom 1990; Raupach et al. 1991), $\sigma_p \sim 6u_*^2$, which is independent of z. We should note that the above arguments are not valid for strongly unstable conditions since $\sigma_w = C_w u_*(1 - 3z/L)^{1/3}$, which depends on $z^{1/3}$. Interestingly, this estimate of σ_p is identical to Kraichnan's (1956a) "mirror-flow" model estimate of C_p ($=\sigma_p/u_*^2$), which he derived without the use of MOS. We note that an order of magnitude estimate can only provide a crude numerical value for C_p.

c. *Townsend's (1961) hypothesis*

Townsend's (1961) hypothesis states that the turbulent eddy motion in the inner region of a boundary layer consists of an "active" part that produces the shear stress τ_0 and whose statistical properties are universal functions of τ_0 and z, and an "inactive" and irrotational part determined by the turbulence in the outer region of the boundary layer. As shown by Raupach et al. (1991), necessary but not sufficient condi-

tions for the validity of Townsend's (1961) hypothesis (as well as MOS) are as follows.

1) A local equilibrium between turbulent production and dissipation must exist.
2) The thickness of this dynamic layer must be much smaller than the total depth of the turbulent boundary layer (h_b) so that the turbulent production and dissipation rates in that layer are independent of eddies of size h_b.
3) The variation of the shear stress across the dynamic layer must be negligible so as not to introduce an additional length scale that characterizes this variation.

Bradshaw (1967) evaluated Townsend's (1961) hypothesis using surface pressure data and found it to be valid for $z/h_b < 0.2$. He attributed the inactive component partly to the irrotational motion due to pressure fluctuations produced in the outer region and partly to the large-scale vorticity field of the outer region turbulence, which the inner region senses as variability in the mean flow. Later, Perry and Abell (1977) and Perry et al. (1986) suggested that the outer region scales with u_* and h_b, while the inner region scales with u_* and z.

d. Low-wavenumber power spectra for p and u

In order to derive the power spectra for the large-scale velocity and turbulent pressure fluctuations and to be consistent with the framework of Kader and Yaglom (1990, 1991), we start with the general dimensional analysis proposed in Kader and Yaglom (1991) for the dynamic sublayer of the ASL:

$$\frac{E_p(K)}{u_*^4 z} = \phi_p(Kz)$$

$$\frac{E_u(K)}{u_*^2 z} = \phi_u(Kz), \tag{8}$$

where $E_p(K)$ and $E_u(K)$ are the power spectral density functions of p and u_1, respectively, and K is the wavenumber along the longitudinal direction. Next we consider the large-scale eddy motion whose sizes are much larger than z and restrict our spectral analysis to $Kz \ll 1$ and $Kh_b \gg 1$. For these wavenumber limits, if Townsend's (1961) hypothesis is valid, the spectra should scale with the outer-region rather than the inner-region variables and should therefore represent the inactive eddy motion (dimensions on the order of h_b) contributing to the dynamic sublayer (recall that the active eddy motion is of size z). Hence, E_p and E_u for the inactive eddy motion ($Kz \ll 1$) must be independent of z (Kader and Yaglom 1991; Raupach et al. 1991). The height independence of the power spectra can only be achieved if

$$\phi_p = \frac{C_{pp}}{Kz}$$

$$\phi_u = \frac{C_{uu}}{Kz}, \tag{9}$$

where C_{pp} and C_{uu} are similarity constants. This leads to -1 power-law expressions for $E_p(K)$ and $E_u(K)$, which are given by

$$E_p(K) = C_{pp} u_*^4 K^{-1}$$

$$E_u(K) = C_{uu} u_*^2 K^{-1}. \tag{10}$$

For E_u the formulation is identical to that obtained by Kader and Yaglom (1991), Kader et al. (1989), Yaglom (1993) for $Kz \ll 1$ and $Kh_b \gg 1$ (see Yaglom 1993, 1994), and Katul et al. (1995b). Although the focus of this study is primarily on the pressure spectra, the velocity spectra are used to independently verify the role of inactive eddy motion. It is interesting to compare the above analysis with the conclusions by Farabee (1986) and the supporting data in Keith et al. (1992) and Keith and Bennett (1991). Based on a spectral solution of (3), Farabee (1986) and Farabee and Casarella (1991) concluded that spectral contributions to p at high frequencies are the result of turbulent velocity fluctuations in the wall region. However, their study showed that the contributions to p at low frequencies are the result of turbulent velocity fluctuations across the entire boundary layer, which is consistent the arguments in Townsend (1976, 165). Clearly, Farabee's (1986) analysis is consistent with the height-independence argument for $Kz \ll 1$. The height independence was also evident in Elliott's (1972b) ground and free air static pressure spectra measurements.

3. Experiment

The experiment was carried out on 10–11 September (DOY = 253–254) 1994 in a 480 m (N–S) × 305 m (E–W) *Alta fescue* grass-covered forest clearing in the Blackwood division of the Duke Forest in Durham, North Carolina (latitude = 38°N, elevation = 163 m). The mean grass height during these two days was 0.4 m. The surrounding trees are 11-m tall southern loblolly pine (*Pinus taeda L*).

In the northwest section of the plot (50 m from west edge and 100 m from north edge), a Gill triaxial sonic anemometer (Gill Instruments, model 1012S), a free air static pressure probe, and a Campbell Scientific krypton hygrometer were collocated at $z = 1.54$ m above the ground surface for measuring U_i, P, and the water vapor density (Q), respectively. The pressure probe and the Krypton hygrometer were situated 30 cm east and west, respectively, of the triaxial sonic anemometer.

The free air static pressure probe used in this study was manufactured by Conklin (1994) using the design of Robertson (1972) and is briefly reviewed in the appendix (see Conklin 1994, pp. 26–28, 93–96 for fur-

ther details). Conklin et al. (1991) compared two free air static pressure designs in the field and in a wind tunnel for performance and ease of construction. The first probe was already manufactured by Sigmon et al. (1983) using the design of Elliott (1972a,b), and the second probe was built at the School of the Environment, Duke University, using the design of Robertson (1972). While neither design showed clear superiority in these comparisons, Conklin (1994) selected the design of Robertson (1972) based on ease of fabrication and uniform response for a wider range of attack angles, as often found at forested sites.

The Gill sonic anemometer was calibrated at the Department of Aeronautics and Astronautics wind tunnel facility (2.1 m × 1.5 m × 4.4 m) at Southampton University and tested for any transducer delays and flow distortions. The sonic pathlength for this unit is 0.149 m. The pathlength for the Campbell Scientific krypton hygrometer is 1.342 cm. The absolute temperature (T), used in determining the sensible heat flux, was computed from the measured speed of sound (c_s) using

$$T = \frac{c_s^2}{\alpha_T R_d}, \tag{11}$$

where $\alpha_T = C_{pa}/C_{va}$ (=1.4), C_{pa} and C_{va} are the specific heat capacities of dry air at constant pressure and volume, respectively, and R_d (=287.04 J kg^{-1} K^{-1}) is the gas constant for dry air. The adequacy of the Gill triaxial sonic anemometer for measuring temperature fluctuations is discussed in Katul (1994) and Katul et al. (1994a,b).

A Campbell Scientific 21X micrologger was used to sample the measured signals at 10 Hz, and the data were transferred to a personal portable computer via a serial input–output optically isolated RS232 interface. The experiment resulted in 26 runs each having a duration of 27.3 minutes (N = 16 384 data points per measured flow variable per run). The mean meteorological and turbulence conditions for all 26 runs are presented in Table 1, where the integral time scales for u_i (=I_{ui}) and p (=I_p), and the Obukhov length (=L_{mo}) were calculated from

$$I_{u_i} = \frac{1}{\langle u_i^2 \rangle} \int_0^\infty \langle u_i(t+\tau) u_i(t) \rangle d\tau; \quad i = 1, 2, 3$$

$$I_p = \frac{1}{\langle p^2 \rangle} \int_0^\infty \langle p(t+\tau) p(t) \rangle d\tau$$

$$L_{mo} = \frac{-\rho u_*^3}{kg\left(\dfrac{H}{c_{pa}T} + 0.61\dfrac{L_v E}{L_v}\right)}, \tag{12}$$

where g (=9.81 m s^{-2}) is the gravitational acceleration, H (=$\rho C_{pa}\langle u_3\theta' \rangle$) is the sensible heat flux, C_{pa} = 1005 J kg^{-1} K^{-1}, L_v (=2.48 × 10^6 J Kg^{-1}) is the latent heat of vaporization, $L_v E$ (=$L_v\langle u_3 q \rangle$) is the latent heat flux, and q (=$Q - \langle Q \rangle$) is the water vapor density fluctuation. In order to compute I_{ui} and I_p from finite datasets (N = 16 384), the integration was carried out to the first zero crossing. Notice from Table 1 that an order of magnitude analysis results in $\langle U_1 \rangle \sim 1$ m s^{-1}, $I_p \sim 10$ s, $I_{u1} \sim 20$ s, and $I_{u3} \sim 1$ s. Hence, the eddy sizes contributing to the vertical motion (=$\langle U_1 \rangle I_{u3}$) are of order z (=1.54 m), while those contributing to the longitudinal motion (=$\langle U_1 \rangle I_{u1}$) and pressure (=$\langle U_1 \rangle I_p$) are of order 10 z. These eddy-size estimates are consistent with Bradshaw's (1967) arguments that the vertical exchange processes scale with z, while the horizontal exchange processes are influenced by the inactive eddy motion in the outer layer. It is interesting to note that these measured velocity length scale ratios $[\langle U_1 \rangle I_{u1}]/[\langle U_1 \rangle I_{u3}] = 20$ are in good agreement with Kader et al. (1989) relations for a neutral ASL ($L_u/L_w = 10.3z/0.5z = 20.6$).

A sample output of the measurements is shown in Fig. 1 for run 3. Notice from Fig. 1 that the large-scale pressure timescales are more compatible with u than with w even for very small $\langle U_1 \rangle$ (see Table 1).

When comparing results with laboratory studies, it is customary to report the roughness Reynolds number R^+ (=$u_* z_0/\nu$) to identify whether the boundary-layer flow regime is hydrodynamically smooth, transitional, or fully rough. For that purpose, it is necessary to estimate the momentum roughness height z_0. A mean z_0 value was obtained by iteratively minimizing the mean squared difference between the predicted $\langle U_1 \rangle$ from

$$\langle U_1 \rangle = \frac{u_*}{k}\left[\ln\left(\frac{z}{z_0}\right) - \Psi_m\left(\frac{z}{L_{mo}}\right)\right]$$

$$\Psi_m\left(\frac{z}{L_{mo}}\right) = 2\ln\left(\frac{1+\chi}{2}\right) + \ln\left(\frac{1+\chi^2}{2}\right) - 2\tan^{-1}(\chi) + \frac{\pi}{2}$$

$$\chi = \left(1 - 16\frac{z}{L_{mo}}\right)^{1/4} \tag{13}$$

and the triaxial sonic anemometer measured $\langle U_1 \rangle$ for all 26 runs. In (26), u_* and z/L_{mo} were measured by the triaxial sonic anemometer, and $\Psi_m(z/L_{mo})$ is the momentum stability correction function presented in Brutsaert (1982, 70). With measured u_*, L_{mo}, and z_0 (=0.10 m), a comparison between predicted and measured $\langle U_1 \rangle$ is carried out in Fig. 2. Good agreement between predictions and measurements is noted, indicating that z_0 = 0.10 m is a valid estimate. Also, this estimate of z_0 is in agreement with other estimates for natural grass surfaces reported in Brutsaert (1982, 115; Table 5.1) and Sorbjan (1989, 68; Table 4.1). For the purpose of this study, we set the zero-plane displacement height to zero. With this estimate of z_0, it is evident that R^+ exceeds 1000. Therefore, the grass-covered surface is hydrodynamically rough and inde-

TABLE 1. Summary of mean meteorological and turbulence conditions. Runs 1–9 are for DOY = 253 (start time = 1135 EST), and runs 10–26 are for DOY = 254 (start time = 1003 EST). The sensible (H) amd latent (L_vE) heat fluxes are also shown.

Run	u_* (m s^{-1})	H (W m^{-2})	L_vE (W m^{-2})	$-z/L_{mo}$	$\langle T \rangle$ (K)	$\langle U_1 \rangle$ (m s^{-1})	I_{u1} (s)	I_{u2} (s)	I_{u3} (s)	I_p (s)
1	0.211	153	240	0.33	301.1	1.21	13.8	18.8	1.0	7.3
2	0.096	145	210	3.26	301.7	0.43	86.9	18.4	2.8	16.2
3	0.126	124	207	1.23	301.9	0.26	65.5	59.7	1.6	19.4
4	0.203	98	226	0.25	301.8	0.71	34.6	67.6	2.6	24.2
5	0.205	87	211	0.22	302.0	0.85	27.6	33.9	2.1	17.2
6	0.233	61	171	0.11	301.5	1.01	18.3	52.9	1.6	5.7
7	0.196	24	140	0.08	300.8	0.71	7.8	44.7	1.7	13.6
8	0.112	22	109	0.40	301.0	0.38	19.5	47.4	2.5	13.5
9	0.067	18	46	1.28	299.9	0.24	22.2	62.2	2.5	20.4
10	0.320	99	134	0.06	296.2	1.72	41.8	41.4	0.6	31.0
11	0.310	119	174	0.08	297.1	1.41	8.5	32.2	0.8	28.8
12	0.293	118	166	0.10	297.9	1.46	24.1	14.6	0.7	9.6
13	0.298	132	207	0.10	298.5	1.40	34.3	43.2	1.0	9.8
14	0.278	134	208	0.13	299.0	1.43	27.5	26.3	0.9	15.6
15	0.323	143	228	0.09	299.5	1.80	19.5	27.3	0.7	17.9
16	0.307	208	312	0.15	300.3	1.10	19.3	18.1	2.3	8.6
17	0.225	154	210	0.27	300.0	0.86	19.8	54.4	0.9	20.8
18	0.251	144	196	0.18	300.4	1.16	19.0	37.6	1.0	27.3
19	0.188	122	193	0.38	300.6	0.52	19.6	41.8	1.2	25.1
20	0.239	112	208	0.17	300.5	1.04	33.9	77.8	0.9	56.0
21	0.288	158	264	0.13	301.3	1.14	70.9	48.2	2.1	25.2
22	0.214	86	153	0.18	300.0	1.01	25.4	18.2	1.6	24.2
23	0.158	37	101	0.20	299.9	0.78	10.8	21.1	1.2	10.9
24	0.164	47	112	0.23	300.1	0.85	18.9	19.1	0.8	19.0
25	0.150	11	83	0.10	298.9	0.66	33.5	14.7	1.4	17.9
26	0.121	4	47	0.08	298.8	0.60	16.6	11.5	1.9	6.5

pendent of R^+ for all 26 runs (Monin and Yaglom 1971, 289).

4. Results and discussion

This section is divided into three parts. The first part discusses some generalities about the dynamic sublayer identification, the second part presents the relationship between σ_p and u_*, and the third part presents the spectral characteristics of pressure fluctuations, large-scale longitudinal eddy motion, and large-scale vertical eddy motion in the dynamic sublayer.

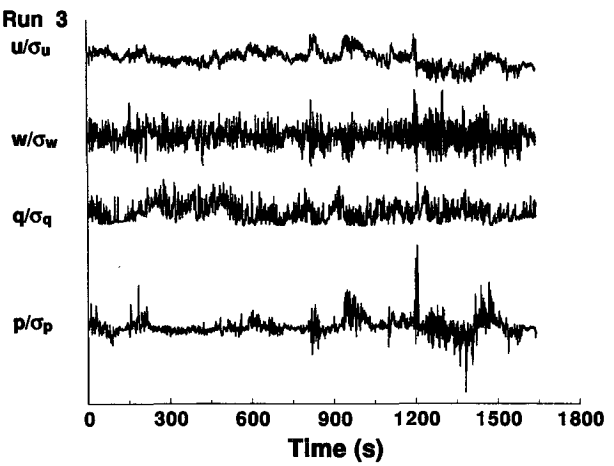

FIG. 1. A sample time variation of the measured normalized longitudinal (u/σ_u) and vertical (w/σ_w) velocity, water vapor density (q/σ_q), and free air static pressure (p/σ_p) fluctuations (run 3).

a. *Identification of the dynamic sublayer*

In theory, the dynamic sublayer occurs only when $-z/L_{mo} = 0$. In practice, a finite but small z/L_{mo} results in an "operational" dynamic sublayer, depending on the purpose of the study. In order to identify this dynamic sublayer, we employ the dimensionless rms for u_3 (to represent vertical motion), the dimensionless rms for u_1 (to represent horizontal motion), and the dimensionless shear stress (to represent the constant stress layer). Figures 3a and 3b show the variation of σ_w/u_* and σ_u/u_* with z/L_{mo}, respectively. In the dynamic sublayer, the stability parameter does not influence the velocity statistics so that σ_w/u_* and σ_u/u_* are constants independent of z/L_{mo}. It appears from Figs. 3a and 3b that the influence of stability on σ_u and σ_w is negligibly small for $-z/L_{mo} \leq 0.2$. In a separate study, it was shown that when the mean wind direction was from the west and northwest, the measurements at the clearing were influenced by the forest and σ_w/u_* was larger than MOS predictions (see Katul et al. 1995a). These runs were not considered in this experiment.

To further check the $-z/L_{mo} \leq 0.2$ stability range, the dimensionless shear stress R_{uw} defined by

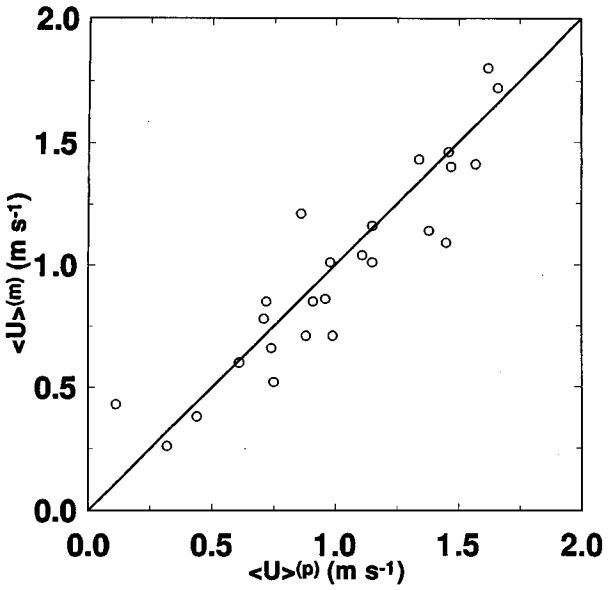

FIG. 2. Comparison between measured and predicted mean longitudinal velocity $\langle U_1 \rangle$ for a momentum roughness length (z_0) = 0.16 m.

$$R_{uw} = \frac{\langle uw \rangle}{\sigma_u \sigma_w} \tag{14}$$

is considered. This stress must also be a constant independent of z/L_{mo} within the dynamic sublayer. Figure 3c displays R_{uw} as a function of $-z/L_{mo}$ and further suggests that R_{uw} is nearly a constant for $-z/L_{mo} \leq 0.2$. From Table 1, we identified 16 runs to be within the dynamic sublayer. This stability limit appears to be a good compromise between minimizing the influence of atmospheric stability on the velocity statistics and maximizing the number of runs in the dynamic sublayer for this experiment.

b. *The rms of the turbulent pressure fluctuations*

It was demonstrated in section 2b that

$$\sigma_p = C_p u_*^2, \tag{15}$$

where C_p is of order unity. From (15), $C_p = 2.4$ was computed by regressing the measured σ_p with the measured u_*^2 and forcing the regression through the origin. Table 2 summarizes the measured C_p for surface-pressure and free air pressure fluctuations for a wide range of laboratory and ASL studies over smooth and rough-wall turbulent boundary layers. We should note that in Table 1, Elliott's (1972a,b) data are the only data collected in the atmosphere, and no atmospheric stability limit was reported. In Fig. 4, a comparison between measured σ_p and predicted σ_p ($=2.4\ u_*^2$) is displayed for all 26 runs. Good agreement between measurements and predictions are noted. Our estimated value for ρC_p ($=1.08$ kg m^{-3} $\times$ 2.4) $\approx$ 2.6 is identical to that of Elliott (1972a,b).

Many experiments on rough and smooth wall turbulent boundary layers result in surprisingly very similar estimates for C_p at the wall and in the free atmosphere. From Table 1, it appears that C_p does not vary appreciably with z, nor does it vary appreciably with the roughness of the surface. Both of these results are consistent with the argument that the main contribution to σ_p is from inactive eddy motion generated in the outer layer. The fact that C_p does not vary appreciably with z close to the ground surface, and the fact that the mean integral length scale is not comparable to z, implies that the main contribution to σ_p is from eddy sizes that do not scale with z. Hence, C_p cannot be significantly affected by the active eddy motion in the dynamic layer. Also, since C_p is similar for rough and smooth turbulent boundary layers, this implies that the details of the boundary roughness elements are not directly responsible for C_p. Hence, the contributions to C_p cannot originate from the viscous sublayer (see Townsend 1976, 168). Therefore, the main contribution to σ_p must be from the inactive eddy motion in the outer layer. This layer is not directly influenced by the surface properties and is only affected by the boundary through u_*. Also, the turbulence statistics in this layer are independent of z. This is consistent with C_p being independent of z and the Eulerian integral timescale analysis presented in section 3.

c. *The large-scale spectral characteristics of the pressure fluctuations*

As discussed in section 2c, for $Kz \ll 1$, $E_u(K)$ and $E_p(K)$ are governed by the inactive motion in the outer layer. Figures 5a and 5b display the normalized longitudinal velocity and pressure spectra as a function of the normalized wavenumber Kz for all runs with $-z/L_{mo} \leq 0.2$. The spectra were calculated by square windowing 8192 data points and cosine tapering the window edges, computing the power spectra for each window, and finally averaging the resultant spectral density functions for each run. Taylor's frozen hypothesis was used to convert the time to the wavenumber domain. An extensive -1 power law is present for $0.02 < Kz < 0.5$ in both figures. We note that the data of Kader and Yaglom (1991) also exhibit a -1 power law with the estimated $C_{uu} = 0.95$. The -1 power law ($=0.95\ [Kz]^{-1}$) is plotted (solid line) in Fig. 5a and is in good agreement with the measurements. Recall from section 4b that if the inactive eddy motion contributes most to σ_p, then it should be possible to estimate C_{pp} from C_p ($=2.4$) using

$$\sigma_p^2 = (C_p u_*^2)^2 = C_p^2 u_*^4 = \int_{K_L}^{K_u} C_{pp} u_*^4 K^{-1} dK = C_{pp} u_*^4 \ln\left(\frac{K_L}{K_u}\right), \tag{16}$$

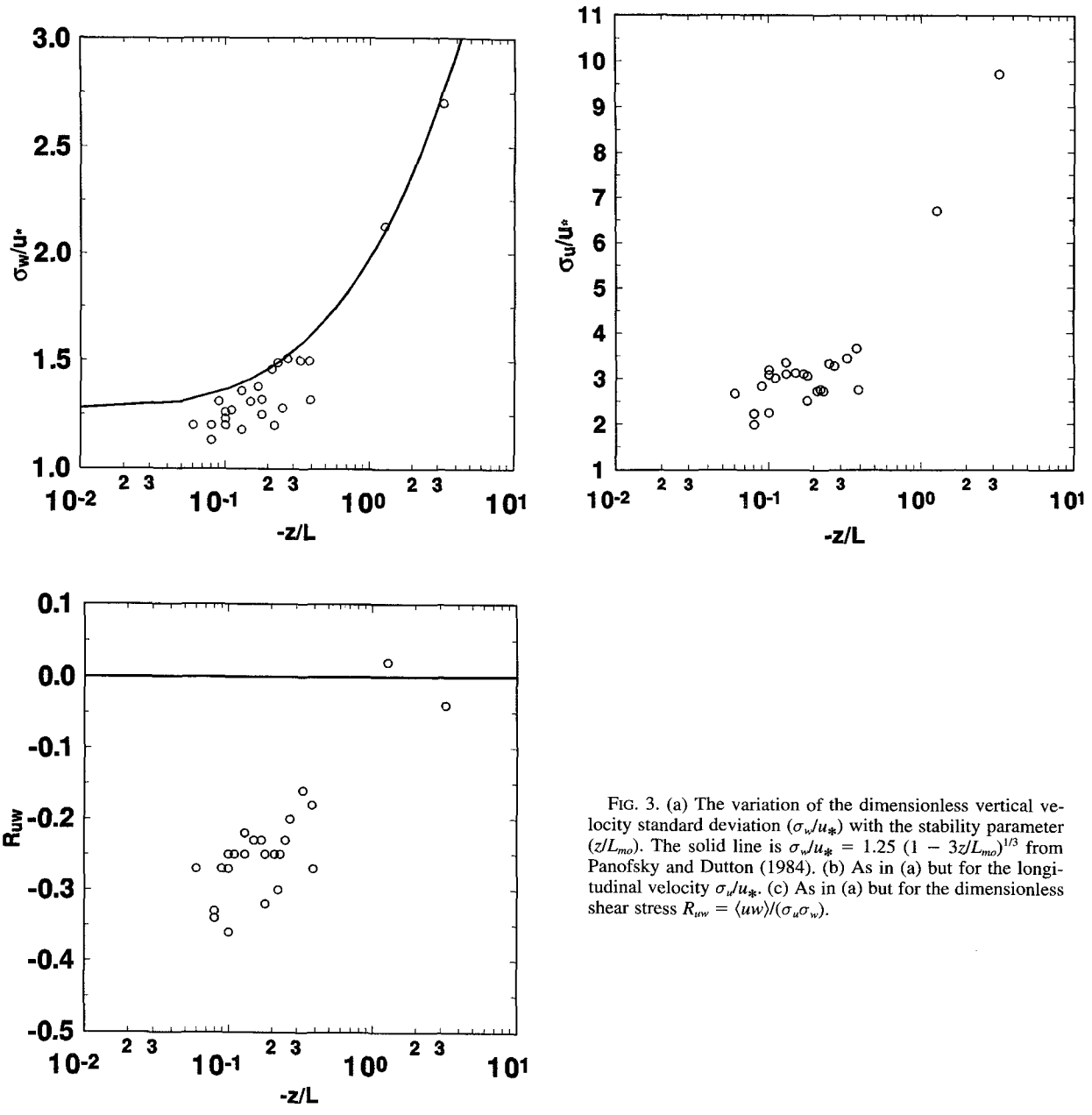

FIG. 3. (a) The variation of the dimensionless vertical velocity standard deviation (σ_w/u_*) with the stability parameter (z/L_{mo}). The solid line is $\sigma_w/u_* = 1.25\ (1 - 3z/L_{mo})^{1/3}$ from Panofsky and Dutton (1984). (b) As in (a) but for the longitudinal velocity σ_u/u_*. (c) As in (a) but for the dimensionless shear stress $R_{uw} = \langle uw \rangle/(\sigma_u \sigma_w)$.

where K_L and K_u define the wavenumber limits of the -1 power law. From Fig. 5b, $K_u/K_L \approx 25$, and thus C_{pp} $(=C_p^2/\ln[K_u/K_L]) \approx 1.7$. The power law 1.7 $(Kz)^{-1}$ (solid line) is also shown in Fig. 5b and is in good agreement with the measurements. The data by Kataoka et al. (1989) and Gorshkov (1967) also exhibit a -1 power law, but no explicit justification was provided by these authors. The wall-pressure spectra measurements in Keith et al. (1992), Farabee and Caseralla (1991), and Keith and Bennett (1991) exhibit an approximate -1 power law for the range of scales corresponding to 0.08–0.5 h_b (these limits are approximate and are estimated by us based on the assumption that the free shear velocity is identical to the convection velocity). We should note that Panton and Linebarger (1974) reported some Reynolds number dependence of E_p in the -1 power law range, and the spectra by Elliott (1972a,b) did not exhibit a -1 but a -0.7 power law (data in Elliott combines unstable and stable runs).

We consider whether C_{pp} could be a universal constant independent of the boundary layer roughness. It appears that (16) and the data in Table 2 suggest that C_p is not a function of surface roughness since C_p did not vary significantly for rough and smooth wall boundary-layer ex-

TABLE 2. The values of ρC_p for surface and free air static pressure in rough and smooth wall turbulent boundary layers. The measured value from this experiment is 2.6.

Reference	ρC_p	Comments
Blake (1970)	2.9–3.8	Wall pressure, smooth and rough boundary layers, measured.
Bull (1967)	2.1–2.5	Wall pressure, smooth wall wind tunnel, measured.
Corcos (1964)	2.1	Wall pressure, turbulent pipe flow, measured.
Elliott (1972a,b)	2.6	Free air, natural surface, measured.
Farabee and Casarella (1991)	2.6–3.1	Wall pressure, wind tunnel, measured.
Kraichnan (1956a,b)	6.0	Estimated by the mirror-flow model.
Willmarth (1975)	2.1–3.1	Wall pressure, rough and smooth wall, measured.
Willmarth and Yang (1970)	2.39–2.8	Wall pressure, axially symmetric and plane boundary layers.
Willmarth and Wooldridge (1962)	2.19	Wall pressure, smooth boundary layer, measured.

periments. An explanation to this roughness boundary invariance might be derived from the behavior of the solution to the Poisson equation away from the boundary. Let us illustrate by using (3), which is written as

$$\frac{\partial^2 p}{\partial x_i \partial x_i} = -\beta(x_i) \Rightarrow p(x_i)$$

$$= \frac{1}{4\pi}\int_D \beta(\alpha_i)\frac{1}{x_i - \alpha_i}\,d\alpha_i + H_{bc}(x_i, \beta(x_i));$$

with

$$\frac{\partial^2 H_{bc}}{\partial x_i \partial x_i} = 0, \qquad (17)$$

where the integration is carried out over the entire flow domain D, and H_{bc} is a harmonic function whose purpose is to insure that the boundary conditions for (17) are satisfied (Warsi 1993, 479–481). It should be noted that (17) is not an explicit solution for p since the velocity field is needed over the entire flow domain. However, for the three-dimensional Poisson equation in (17), an important property of H_{bc} is its rapid decay with distance from the boundary (Greenberg 1978, 579–595; it should be pointed out that for a two-dimensional laplace equation, the decay of H_{bc} with distance from the boundary is logarithmic and much slower than the three-dimensional case). The rapid decay of H_{bc} does suggest that the influence of the boundary condition details is restricted to a small portion of the flow domain that is in close proximity to the boundary. Away from the boundary, the pressure must become independent of the boundary roughness variations.

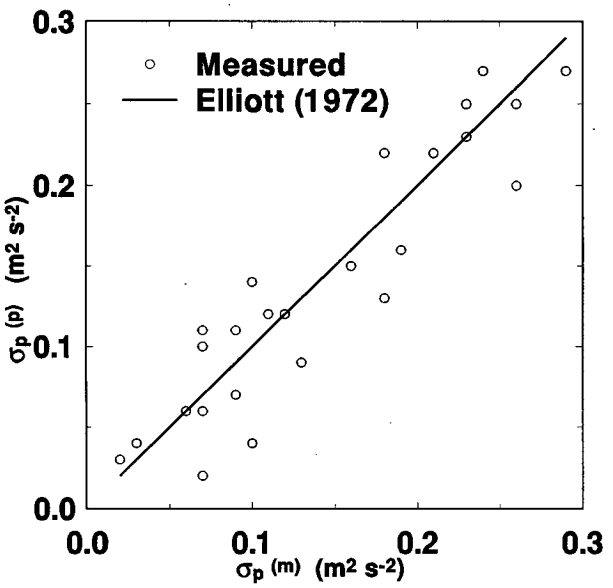

FIG. 4. A comparison between measured ($\sigma_p^{(m)}$) and predicted ($\sigma_p^{(p)}$) root-mean static pressure for all 26 runs. Here $\sigma_p^{(p)} = 2.4u_*^2$. The solid line is from Elliott's (1972a,b) data adjusted by the air density.

The important comment by Townsend (1961) and Bradshaw (1967) regarding the negligible influence of the inactive eddy motion on the vertical transport must be carefully reevaluated in light of recent studies by Högtsröm (1990) and Smedman (1991). Högtsröm (1990) suggested that the inactive turbulence does contribute to the vertical motion in dynamic sublayer. He attributed the contribution of the inactive eddy motion to the variation of σ_w/u_* with z. Smedman (1991) also found that Högtsröm's (1990) data is in agreement with near-neutral σ_w/u_* and σ_u/u_* surface-layer measurements at five sites. Whether the inactive eddy motion contributes to the vertical motion appears to be unclear (see Yaglom 1993). We note that the variation in σ_w/u_* measured by Smedman (1991) is only between 1.15 and 1.3 for all five sites.

If the inactive eddy motion significantly influences the vertical transport, then the spectrum of the vertical velocity $E_w(K)$ should be, to a first approximation, similar to $E_u(K)$ for $Kz \ll 1$. That is, $E_w(K) = C_{ww}u_*^2K^{-1}$ could be derived as was earlier done for the longitudinal velocity using the height independence arguments. The dimensionless vertical velocity power spectrum is shown in Fig. 5c as a function of the dimensionless wavenumber. In contrast to Figs. 5a and 5b, it is evident from Fig. 5c that a -1 power law does not

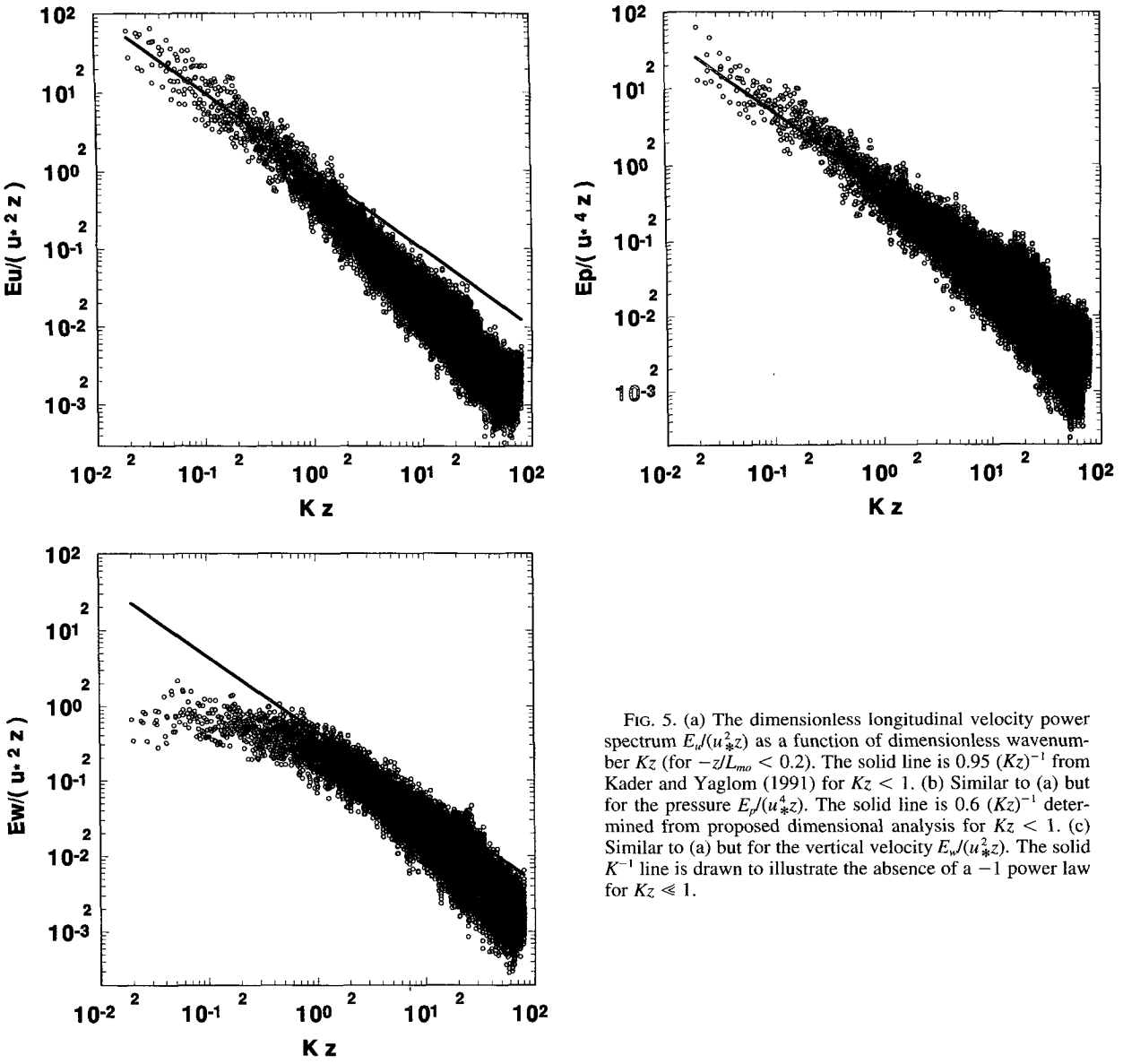

FIG. 5. (a) The dimensionless longitudinal velocity power spectrum $E_u/(u_*^2 z)$ as a function of dimensionless wavenumber Kz (for $-z/L_{mo} < 0.2$). The solid line is 0.95 $(Kz)^{-1}$ from Kader and Yaglom (1991) for $Kz < 1$. (b) Similar to (a) but for the pressure $E_p/(u_*^4 z)$. The solid line is 0.6 $(Kz)^{-1}$ determined from proposed dimensional analysis for $Kz < 1$. (c) Similar to (a) but for the vertical velocity $E_w/(u_*^2 z)$. The solid K^{-1} line is drawn to illustrate the absence of a -1 power law for $Kz \ll 1$.

exist for $Kz \ll 1$. We note that Kader and Yaglom (1991), Katul et al. (1995b), and Katul and Parlange (1995) did measure a short -1 power law for E_w in the unstable ASL; however, these measurements were restricted to $Kz > 0.3$ and thus cannot be the result of the larger-scale inactive eddy motion.

The arguments regarding the role of the inactive eddy motion in the inner region is also in agreement with earlier ASL measurements presented in Panofsky and Dutton (1984, 160–168). The data in Panofsky and Dutton (1984) clearly demonstrate that σ_w scales with z/L_{mo}, while σ_u does not for the unstable ASL. The authors found that σ_u is independent of z and scales with h_b/L_{mo}. The fact that σ_u is dependent on h_b further suggests that the inactive eddy motion in the outer layer governs the horizontal transport statistics (see also Gifford 1989). Panofsky and Dutton's (1984) data are also consistent with Fig. 5a, for which E_u was derived using the height-independence argument. We note that the range $Kz < 0.5$ contributes, on average, to 90% of the variance of u for the 16 runs.

d. *Further comments on E_u and E_w at low wavenumbers*

The possibility that the large scales in wall-bounded shear flow possess a universal spectral behavior is not new and was first proposed by Tchen (1953). Tchen (1953) noted that the interaction between the large-scale eddies and the mean flow is controlled by the

terms involving $u_i\langle U_j\rangle$ and $u_j\langle U_i\rangle$. He concluded that the spectrum of u_1 is proportional to K^{-1} when the vorticity of the mean flow is large and interacting with the turbulent motion. It is interesting to compare the similarities in Tchen's (1953) arguments with those of Kraichnan (1956a,b) and Townsend (1961), as utilized in the above derivation. Later, Klebanoff (1954) conducted experiments in a boundary layer along a smooth flat plate with zero pressure gradient. His results support Tchen's (1953) predictions for the u_1 spectrum (E_u) at low wavenumbers, especially for $z/h_b \sim 0.05$ (see also Hinze 1959, 501). It is noted that in Klebanoff's (1954) experiments, E_u did not exhibit a -1 power law for $z/h_b = 0.0011$ and $z/h_b = 0.8$. Hinze (1959) suggests that the -1 power law occurs in the proximity of the wall boundary, yet far enough away so that viscous effects have negligible influence on the large scales. Interestingly enough, Hinze (1959) proposed that at $z/h_b = 0.05$ strong production of turbulence energy takes place by turbulence–mean flow interaction. As z/h_b decreases, the contribution of larger eddies to the turbulent energy reduces at the low wavenumber end but increases at the high wavenumber end of the energy spectrum. Experiments for turbulent air flow in pipes by Perry and Abell (1975) focused on the scaling properties of E_u in the overlap region between the "inner flow" and "outer flow." The logarithmic mean velocity profile, originally derived by Izakson (1937) and used by Millikan (1939) to arrive at the Prandtl–Nikuradse skin friction law (see Monin and Yaglom 1971, 299), exists in this region. Perry and Abell (1975) found that E_u is proportional to K^{-1} for low wavenumbers but that E_w is not, which is in agreement with the present results. This was independently confirmed by Korotkov (1976) using channel flow data. Raupach et al. (1991) and Antonia and Raupach (1993) discussed the existence of a -1 power law scaling for E_u and E_w in rough wall boundary layers but argued against its existence in the ASL based on the Kansas experiments reported in Kaimal et al. (1972). They attributed the general absence of a K^{-1} scaling to the buoyancy effects in the ASL that are absent in the outer region of many laboratory boundary layers. Further details on other studies can be found in Yaglom (1993, 1994), Katul and Parlange (1995), and Katul et al. (1995b). All these results appear to support the present arguments regarding the role of the inactive eddy motion in the dynamic sublayer.

5. Conclusions

The large-scale structure of the pressure field was investigated using measured static pressure fluctuations in the dynamic sublayer over a grass-covered forest clearing. The boundary was shown to be hydrodynamically rough for all runs during the experiment. Our results demonstrate the following.

1) The inactive eddy motion in the outer region of the atmospheric boundary dominates the large-scale statistical structure of the turbulent static pressure and longitudinal velocity fluctuations. This conclusion supports Townsend's (1961) hypothesis, Bradshaw's (1967) analysis, and Tchen's (1953) arguments.

2) The Eulerian integral timescale for the pressure is an order of magnitude larger than that of the vertical velocity. This result demonstrates that the eddy sizes contributing to the pressure internal correlation are larger than z in the dynamic sublayer. The Eulerian length scales for vertical velocity, as derived from the Eulerian timescales and Taylor's hypothesis, are very close to z. This conclusion is consistent with the role of active–inactive eddy motion in the dynamic sublayer in the longitudinal and vertical directions.

3) The ratio of the root-mean-square pressure fluctuations and the squared friction velocity (C_p) at the ground and in the free atmosphere were found to be very similar for rough and smooth boundary-layer flows. This indicates that, to a first approximation, C_p is a constant independent of height and surface roughness. Our experimentally derived value for C_p closely resembles values derived from laboratory wall pressure measurements reviewed by Willmarth (1975).

4) The low-wavenumber spectral properties of the pressure for eddy sizes much larger than the measurement height ($Kz \ll 1$) follow a well defined -1 power law. The only dynamic parameter influencing this spectrum is u_*. Based on the integral representation of the Poisson equation for p, it was demonstrated that the wall boundary roughness does not influence the statistical properties in the outer region. A conclusion derived from this argument is that the similarity constant C_{pp}, for the low-wavenumber pressure spectrum, is independent of the boundary-layer roughness.

5) The inactive eddy motion does not contribute to the vertical exchange processes as evidenced by the vertical velocity power spectrum in the dynamic sublayer, thus reinforcing the well-established similarity formulations for vertical velocity.

Acknowledgments. The authors would like to thank Professors Akiva Yaglom and Douglas Lilly for their comments and suggestions, and Judd Edeburn for his help at the Duke Forest. This project was supported, in part, by the Environmental Protection Agency under the cooperative agreement 91-0074-94 (CR817766) and the National Science Foundation through Grants BIR-9512333 and ATM-7825944, and the NASA graduate fellowship in Global Climate Change Research Program.

APPENDIX

Pressure Probe Details

Although much of this material is discussed in great details by Conklin (1994), we present the main ele-

ments of the pressure sensor design. The free air pressure sensor was manufactured by P. Conklin at the School of the Environment (Duke University) following the design of Robertson (1972). Conklin et al. (1991) carried out a wind tunnel and in situ comparison of the probe designed by Robertson and another probe manufactured by Sigmon et al. (1983) following the design of Elliott (1972a). While Conklin et al. (1991) concluded that neither design showed clear superiority, they suggested the use of the design of Robertson for ease of fabrication. This design consists of 15-cm diameter parallel flat plates separated by 10 cm. The aluminum plates are $1/16$ inch thick with brass fittings threaded into each plate for the 2-mm pressure transducer ports. The fittings were machined flush with the surface. The inside surface of each plate was then polished. The pressure probe was attached by a 65-cm long tube to a Datametrics model 570D-10B-2A1-V1X Barocell pressure transducer. The capacitance output from this transducer was converted to an analog voltage signal in the instrument using a model 1015-A4C-12A1-G electronic manometer. The pressure transducer reference was connected to a 1-L vacuum insulated flask that is vented to the atmosphere by a long capillary tube. In essence, the reference flask acts as a low-pass filtered reference that efficiently removes synoptic-scale pressure changes (see, e.g., Kataoka et al. 1989). The capillary tube time constant was measured from a first-order exponential response curve to be 11.2 minutes.

To determine the response of the probe to horizontal and vertical rotations, the probe was installed in a laminar boundary-layer wind tunnel (cross section is 1.5 m $\times$ 1.5 m). A pitot tube situated upstream of the pressure probe was connected to the reference side of the pressure transducer so that differences between the two readings are directly monitored. The pressure probe had a constant response for wind attack angles up to 20° and three wind speeds of 3, 5, and 10 m s^{-1}. The response of the probe was invariant to horizontal rotations for all three wind speeds.

REFERENCES

Antonia, R. A., and M. R. Raupach, 1993: Spectral scaling laws in a high Reynolds number laboratory boundary layer. *Bound.-Layer Meteor.*, **65,** 289–306.

Batchelor, G. K., 1953: *The Theory of Homogeneous Turbulence.* Cambridge University Press, 197 pp.

Blake, W. K., 1970: Turbulent boundary-layer wall-pressure fluctuations on smooth and rough walls. *J. Fluid Mech.*, **44,** 637–660.

Bradshaw, P., 1967: Inactive motion and pressure fluctuations in turbulent boundary layers. *J. Fluid Mech.*, **30,** 241–258.

Brutsaert, W., 1982, *Evaporation into the Atmosphere: Theory, History, and Applications.* Kluwer Academic Publishers, 299 pp.

Bull, M. K., 1967: Wall-pressure fluctuations associated with subsonic turbulent boundary layer flow. *J. Fluid Mech.*, **28,** 719–754.

Conklin, P. S., 1994: Turbulent wind temperature and pressure in a mature hardwood canopy. Ph.D. dissertation, Duke University, 105 pp. [Available from School of the Environment, Duke University, Durham, NC 27908-0328.]

——, K. R. Knoerr, and C. B. Baker, 1991: A wind tunnel and field comparison of two static pressure probes. Preprints, *Seventh Symp. on Meteorological Measurements and Instrumentation,* New Orleans, LA, Amer. Meteor. Soc., 92–95.

Corcos, G. M., 1963: Resolution of pressure in turbulence. *J. Acoust. Soc. Am.*, **35,** 192–199.

——, 1964: The structure of the turbulent pressure field in boundary-layer flows. *J. Fluid Mech.*, **23,** 353–378.

Elliott, J. A., 1972a: Instrumentation for measuring static pressure fluctuations within the atmospheric boundary layer. *Bound.-Layer Meteor.*, **2,** 476–495.

——, 1972b: Microscale pressure fluctuations measured within the lower atmospheric boundary layer. *J. Fluid Mech.*, **53,** 351–383.

Farabee, T. M., 1986: An experimental investigation of wall pressure fluctuations beneath non-equilibrium turbulent flows. DTNSRDC Tech. Rep. 86/047, 51 pp. [Available from Dr. T. Farabee, David Taylor Research Center, Bethesda, MD 20084.]

——, and M. J. Casarella, 1991: Spectral features of wall pressure fluctuations beneath turbulent boundary layers. *Phys. Fluids A,* **3,** 2410–2420.

Garratt, J. R., 1992: *The Atmospheric Boundary Layer.* Cambridge Atmospheric and Space Science Series, Cambridge University Press, 316 pp.

George, W. K., P. D. Beuther, and R. E. Arndt, 1984: Pressure spectra in turbulent free shear flows. *J. Fluid Mech.*, **148,** 155–191.

Gifford, F. A., 1989: Does atmospheric turbulence have an outer scale? *Agric. Forest Meteor.*, **47,** 155–161.

Gorshkov, N. F., 1967: Measurements of the spectrum of pressure micropulsations in near-earth layer of the atmosphere. *Izv. Acad. Sci. USSR, Atmos. Oceanic Phys.*, **3,** 447–451.

Greenberg, M. D., 1978: *Foundations of Applied Mathematics.* Prentice Hall, 626 pp.

Hill, R. J., and J. M. Wilczak, 1995: Pressure structure functions for locally isotropic turbulence. *J. Fluid Mech.*, **296,** 247–269.

Hinze, J. O., 1959: *Turbulence.* McGraw-Hill, 586 pp.

Högström, U., 1990: Analysis of turbulence in the surface layer with a modified similarity formulation for near neutral conditions. *J. Atmos. Sci.*, **47,** 1949–1972.

Izakson, A., 1937: Formula for the velocity distribution near a wall. *Zh. Eksp. Teor. Fiz.*, **7,** 919–924.

Kader, B. A., and A. M. Yaglom, 1990: Mean fields and fluctuation moments in unstably stratified turbulent boundary layers. *J. Fluid Mech.*, **212,** 637–662.

——, and ——, 1991: Spectra and correlation functions of surface layer turbulence in unstable thermal stratification. *Turbulence and Coherent Structures,* O. Metais and M. Lesieur, Eds., Kluwer Academic Press, 388–412.

——, ——, and S. L. Zubkovskii, 1989: Spatial correlation functions of surface-layer atmospheric turbulence in neutral stratification. *Bound.-Layer Meteor.*, **47,** 233–249.

Kaimal, J. C., J. C. Wyngaard, Y. Izumi, and O. R. Cote, 1972: Spectral characteristics of surface layer turbulence. *Quart. J. Roy. Meteor. Soc.*, **98,** 563–589.

Kataoka, T., Y. Mitsuta, and O. Tsukamoto, 1989: The development of a fast response static pressure instrument for field use. *J. Meteor. Soc. Japan,* **67,** 351–356.

Katul, G. G., 1994: A model for sensible heat flux probability density function for near-neutral and slightly-stable atmospheric flows. *Bound.-Layer Meteor.*, **71,** 1–20.

——, and M. B. Parlange, 1994: On the active role of temperature in surface-layer turbulence. *J. Atmos. Sci.*, **51,** 2181–2195.

——, and ——, 1995: The spatial structure of turbulence at production wavenumbers using orthonormal wavelets. *Bound.-Layer Meteor.*, **74,** 81–108.

——, J. D. Albertson, M. B. Parlange, C. R. Chu, and H. Stricker, 1994a: Conditional sampling, bursting, and the intermittent

structure of sensible heat flux. *J. Geophys. Res.*, **99,** 22 869–22 876.

——, M. B. Parlange, and C. R. Chu, 1994b: Intermittency, local isotropy, and non-Gaussian statistics in atmospheric surface layer turbulence. *Phys. Fluids,* **6,** 2480–2492.

——, S. M. Goltz, C. I. Hsieh, Y. Cheng, F. Mowry, and J. Sigmon, 1995a: Estimation of surface heat and momentum fluxes using the flux-variance method above uniform and non-uniform terrain. *Bound.-Layer Meteor.,* **74,** 237–260.

——, C. R. Chu, M. B. Parlange, J. D. Albertson, and T. A. Ortenburger, 1995b: The low-wavenumber spectral characteristics of turbulent velocity and temperature in the unstable atmospheric surface layer. *J. Geophys. Res.,* **100,** 14 243–14 255.

Keith, W. L., and J. C. Bennet, 1991: Low-frequency spectra of the wall shear stress and wall pressure in a turbulent boundary layer. *AIAA J.,* **29,** 526–530.

——, D. A. Hurdis, and B. M. Abraham, 1992: A comparison of turbulent boundary layer wall-pressure spectra. *J. Eng. Fluids,* **114,** 338–347.

Klebanoff, P. S., 1954: Characteristics of turbulence in a boundary layer with zero-pressure gradient. Rep. 1247, National Advisory Committee for Auronautics, National Bureau of Standards, Washington DC, 19 pp.

Kolmogorov, A. N., 1941: The local structure of turbulence in incompressible viscous fluid for very large Reynolds numbers. *Dok. Akad. Nauk SSSR,* **30,** 301–304.

Korotkov, B. N., 1976: Some types of local self-similarity of the velocity field of wall turbulent flows. *Izv. Akad. Nauk SSSR, Ser. Mekh. Zhidk. i. Gaza,* **6,** 35–42.

Kraichnan, R. H., 1956a: Pressure field within homogeneous anisotropic turbulence. *J. Acoust. Soc. Am.,* **28,** 64–72.

——, 1956b: Pressure fluctuations in turbulent flow over a flat plate. *J. Acoust. Soc. Am.,* **28,** 378–390.

McBean, G. A., and J. A. Elliott, 1975: The vertical transports of kinetic energy by turbulence and pressure in the boundary layer. *J. Atmos. Sci.,* **32,** 753–766.

——, and ——, 1978: The energy budgets of the turbulent velocity components and the velocity-pressure gradient interactions. *J. Atmos. Sci.,* **35,** 1890–1899.

Millikan, C. B., 1939: A critical discussion of turbulent flow in channels and circular tubes. *Proceedings of the Fifth International Congress on Applied Mechanics,* Wiley, 386–392.

Monin, A. S., and A. M. Obukhov, 1954: Basic laws of mixing in the ground layer of the atmosphere. *Tr. Geofiz Inst., Akad. Nauk SSSR,* **151,** 163–187.

——, and A. M. Yaglom, 1971: *Statistical Fluid Mechanics.* Vol. I. MIT Press, 769 pp.

Panofsky, H. A., and J. Dutton, 1984: *Atmospheric Turbulence: Models and Methods for Engineering Applications,* Wiley and Sons, 397 pp.

Panton, R. L., 1984: *Incompressible Flow.* Wiley and Sons, 779 pp.

——, and J. H. Linebarger, 1974: Wall pressure spectra calculations for equilibrium boundary layers. *J. Fluid Mech.,* **65,** 261–275.

Perry, A. E., and C. J. Abell, 1975: Scaling laws for pipe flow turbulence. *J. Fluid Mech.,* **67,** 257–271.

——, and ——, 1977: Asymptotic similarity of turbulence structures in smooth- and rough-walled pipes. *J. Fluid Mech.,* **79,** 785–799.

——, S. Henbest, and M. S. Chong, 1986: A theoretical and experimental study of wall turbulence. *J. Fluid Mech.,* **165,** 163–199.

Raupach, M. R., R. A. Antonia, and S. Rajagopalan, 1991: Rough-wall turbulent boundary layers. *Appl. Mech. Rev.,* **44,** 1–25.

Robertson, P., 1972: A direction-insensitive static head sensor. *J. Phys. E: Sci. Instrum.,* **5,** 1080–1082.

Schols, J. L., and L. Wartena, 1986: A dynamical description of turbulent structures in the near neutral atmospheric surface layer: The role of static pressure fluctuations. *Bound.-Layer Meteor.,* **34,** 1–15.

Shaw, R. H., and X. J. Zhang, 1992: Evidence of pressure-forced turbulent flow in a forest. *Bound.-Layer Meteor.,* **58,** 273–288.

Sigmon, J. T., K. R. Knoerr, and E. J. Shaughnessy, 1983: Microscale pressure fluctuations in a mature deciduous forest. *Bound.-Layer Meteor.,* **27,** 345–358.

Smedman, A. S., 1991: Some turbulence characteristics in stable atmospheric boundary layer flows. *J. Atmos. Sci.,* **48,** 856–868.

Snarski, S., and R. Lueptow, 1995: Wall pressure and coherent structures in a turbulent boundary layer on a cylinder in axial flow. *J. Fluid Mech.,* **286,** 137–171.

Sorbjan, Z., 1989: *Structure of the Atmospheric Boundary Layer.* Prentice Hall, 317 pp.

Tchen, C. M., 1953: On the spectrum of energy in turbulent shear flow. *J. Res. Nat. Bur. Stand. (US),* **50,** 51–62.

Tennekes, H., and J. L. Lumley, 1972: *A First Course in Turbulence.* MIT Press, 300 pp.

Thomas, A. S. W., and M. K. Bull, 1983: On the active role of wall-pressure fluctuations in deterministic motions in the turbulent boundary layer. *J. Fluid Mech.,* **128,** 283–332.

Townsend, A. A., 1961: Equilibrium layers and wall turbulence. *J. Fluid Mech.,* **11,** 97–120.

——, 1976: *The Structure of Turbulent Shear Flow.* Cambridge University Press, 429 pp.

Warsi, Z. U. A., 1993: *Fluid Dynamics: Theoretical and Computational Approaches.* CRC Press, 683 pp.

——, and C. E. Wooldridge, 1962: Measurements of the fluctuating pressure at the wall beneath a thick turbulent boundary layer. *J. Fluid Mech.,* **13,** 187–210.

——, and C. S. Yang, 1970: Wall-pressure fluctuations beneath turbulent boundary layers on a flat plate and cylinder. *J. Fluid Mech.,* **41,** 47–80.

Willmarth, W. W., 1975: Pressure fluctuations beneath turbulent boundary layers. *Ann. Rev. Fluid Mech.,* **7,** 13–38.

Wyngaard, J. C., and O. R. Cote, 1971: The budgets of turbulent kinetic energy and temperature variance in the atmospheric surface layer. *J. Atmos. Sci.,* **28,** 190–201.

——, A. Siegel, and J. M. Wilczak, 1994: On the response of a turbulent-pressure probe and the measurement of pressure transport. *Bound.-Layer Meteor.,* **69,** 379–396.

Yaglom, A. M., 1979: Similarity laws for constant pressure and pressure-gradient turbulent wall flows. *Ann. Rev. Fluid Mech.,* **11,** 505–541.

——, 1993: Similarity laws for wall turbulent flows: Their limitations and generalizations. *New Approaches and Concepts in Turbulence, Proceedings of the Centro Stefano Franscini Ascona,* Birkhauser Verlag Basel, 7–27.

——, 1994: Fluctuation spectra and variances in convective turbulent boundary layers: A reevaluation of old models. *Phys. Fluids,* **6,** 962–972.